Proceedings of the 17th World Congress
The International Federation of Automatic Control
Seoul, Korea, July 6-11, 2008

Wheelslide and Wheelskid Protection for a Single-Wheel Drive and Brake Module (SDBM) for Rail Vehicles

Thorsten Stützle * **Thomas Engelhardt** * **Manfred Enning** *
Dirk Abel *

* *Institute of Automatic Control (IRT), RWTH Aachen University, Germany (www.irt.rwth-aachen.de).*

Abstract: In this paper, the dynamic behaviour of a rail vehicle with single-wheel drive and brake modules is analysed. It is shown that in the wheelslide or wheelskid case, the linearised plant obtains an unstable pole whose location is determined by the shape of the current creep force curve. By considering possible variations in the shape of the creep force curve, the corresponding variation of the pole location in the right-half plane is calculated and a controller structure for creepage control and creep velocity control is suggested. If the controller design takes the worst-case pole location into account, the resulting controller stabilises the closed loop even at small velocities. Finally, this fact is illustrated through simulation results.

Keywords: Modeling and simulation of transportation systems; Simulation.

1. INTRODUCTION

An improvement with respect to the state-of-the-art of traction systems for rail vehicles is expected from the integration of the functionalities driving and braking into a single mechatronic traction module with a few precisely defined mechanical, electrical and data interfaces. Thus, the railway industry is currently developing and successfully testing an integrated traction drive system called Syntegra™, which consists of a gearless drive based on a high-torque permanent magnet motor [Ger06]. In the Syntegra™ concept, the gearless drive is mounted on a wheelset axle which is rigidly connected to both wheels of the wheelset.

But the degree of modularisation of an integrated traction drive system can be even further increased, if the focus is set on the single wheel instead of the entire wheelset. This consideration leads to the so-called single-wheel drive and brake module (SDBM) whose driving and braking components are integrated into a single wheel (wheel hub motor). By breaking up the rigid connection between the two wheels (or SDBMs) of a wheelset, the opportunity is gained for a reduction of wear and noise as well as an improvement of the driving comfort. At the RWTH Aachen University, four institutes (IFS, IFAS, ISEA, IRT) are currently investigating the SDBM in a joint research project which is funded by the DFG (German Research Foundation). Figure 1 shows the current design stage of the SDBM.

The SDBM consists of a single wheel with a switched reluctance drive and a hydraulic brake. In the joint research project, the task of the Institute of Automatic Control is to design wheelslide and wheelskid protection controllers for an optimal creep force utilisation.

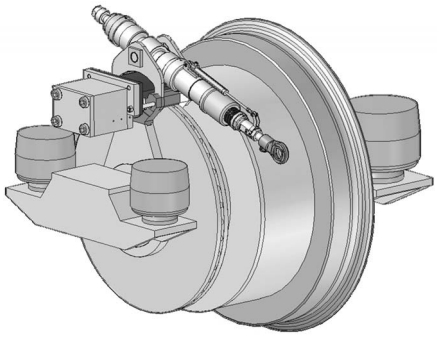

Fig. 1. Current design stage of the SDBM [Her07]

This paper presents the results of a dynamic analysis of the SDBM-wheelslide and wheelskid protection problem which is based on a set of mathematical models. It follows primarily the approach already introduced in [Stü06] but extends it about the consideration of the wheelskid case, the treatment of the creep velocity control task and the use of the well-known POLACH-creep force curve. From that, a structure for creepage and creep velocity controllers is suggested, that is applicable with respect to the wheelslide and wheelskid protection task. Finally, simulation results are shown.

2. WHEELSLIDE AND WHEELSKID PROTECTION

Figure 2 shows the non-dimensional creep force f_x with the maximum value $\mu_{\max}$ as a non-linear function of the longitudinal creepage s. When a brake torque is applied at the wheel, a longitudinal creepage s occurs in the wheel-rail contact region and with this a creepage dependent creep force which decelerates the vehicle. The non-dimensional creep force f_x is the ratio of the creep force to the normal force. Bad frictional conditions reduce the maximum

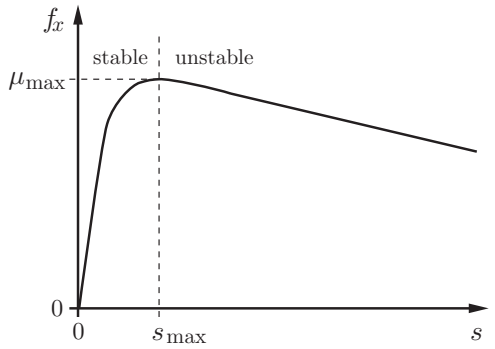

Fig. 2. Non-dimensional creep force vs. longitudinal creepage

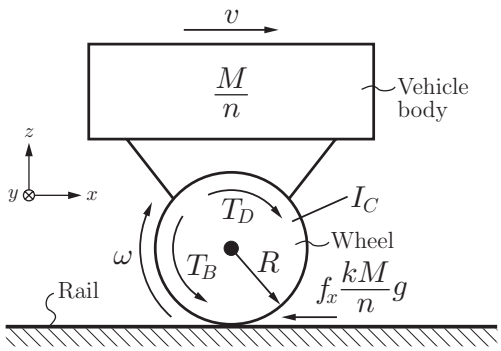

Fig. 3. The nth part vehicle model

considerably. When the maximum is exceeded due to a too high brake torque, the braking becomes unstable - the wheel decelerates much faster than the vehicle and tends to lock up. A similar scenario occurs, when a driving torque is applied at the wheel. If the driving torque is chosen too high, the wheel will start to skid which leads directly to strong wear of the wheel and the rail.

A modern wheelslide protection system must in all cases prevent a wheel lock-up. In addition, it has to ensure that the vehicle brakes within acceptable braking distances. The primary task of a wheelskid protection system is to avoid wheel skidding. At the same time, it should always guarantee an adequate vehicle acceleration.

In order to obtain acceptable braking distances, [UIC05] states that the longitudinal creepage should be greater than 0.1 during most of the braking time. This means that the controller must hold operating points on the decreasing branch of the non-dimensional creep force curve. Experience shows that the same requirement must be fulfilled in order to obtain a reasonable acceleration in the wheelskid protection case. In the following the dynamics of sliding and skidding are considered with the help of mathematical models.

3. MATHEMATICAL MODELS

3.1 Vehicle Model

First of all, a very simple vehicle model is established that can be used for further investigations on the dynamics and the controller design. In the following, the nth part vehicle model for vehicles with n SDBMs shown in figure 3 is considered. The model is based on the so-called quarter vehicle model which is often used in connection with the design of anti-lock brake systems in automobiles, see e.g. [Wu98]. Setting up Newton's equation of motion for the nth part vehicle model results in:

$$\begin{aligned}\dot{v} &= \frac{n}{M}\left[-f_x \frac{M}{n} g\right] \\ &= -f_x\, g\,, \end{aligned} \tag{1}$$

$$\dot{\omega} = \frac{1}{I_C}\left[R f_x \frac{kM}{n} g + T_D - T_B\right]. \tag{2}$$

In these equations, M is the vehicle mass, I_C is the SDBM's moment of inertia, R is the nominal wheel radius, T_D is the driving torque, T_B is the brake torque, and f_x is the available non-dimensional creep force in x-direction. The acceleration of gravity is denoted by g. A change in the normal force that might occur during braking due to the pitching of the vehicle is considered by the factor k.

The creep velocity v_s is the difference between the vehicle velocity v and the wheel circumference velocity $R\,\omega$

$$v_s = v - R\,\omega\,. \tag{3}$$

By relating the creep velocity v_s to the vehicle velocity v, the non-linear creepage relationship is gained

$$s = \frac{v_s}{v} = \frac{v - R\,\omega}{v} = \frac{\frac{v}{R} - \omega}{\frac{v}{R}}\,. \tag{4}$$

In this particular definition of the creepage, the value of s equals 0 if the SDBM-wheel is purely rolling. When braking, the wheel is slipping and the creepage values lie in a range between 0 and 1. Full sliding (or a wheel lock-up) occurs for $s = 1$. During driving, the creepage becomes negative. Skidding means that s tends towards great negative values. Note that s is only defined for $v > 0$ and $\omega \geq 0$.

The derivative with respect to time of equation (3) yields

$$\dot{v}_s = \dot{v} - R\,\dot{\omega}\,. \tag{5}$$

The insertion of equation (1) and equation (2) into equation (5) results in

$$\dot{v}_s = -f_x\, g\left(1 + \frac{R^2 kM}{I_C n}\right) - \frac{R}{I_C}\left(T_D - T_B\right). \tag{6}$$

Due to the non-linear relationship between v_s and f_x, equation (6) represents a non-linear differential equation for the creep velocity dynamics.

The derivative with respect to time of equation (4) writes

$$\dot{s} = \frac{1}{v}\left[\dot{v}\,(1 - s) - R\,\dot{\omega}\right]. \tag{7}$$

Inserting equation (1) and equation (2) into equation (7) yields

$$\begin{aligned}\dot{s} = \frac{1}{v}\Bigg[-f_x\, g\left(1 + \frac{R^2 kM}{I_C n} - s\right) \\ - \frac{R}{I_C}\left(T_D - T_B\right)\Bigg]. \end{aligned} \tag{8}$$

With this, a non-linear differential equation for the creepage dynamics is obtained. The so-called rotation factor λ,

which is a common number in the field of railway vehicle design, has the following definition for the case of the nth part vehicle model

$$\lambda = 1 + \frac{I_C n}{M R^2} \,. \tag{9}$$

With λ, equations (6) and (8) become

$$\dot{v}_s = -f_x\, g \left(1 + \frac{k}{\lambda - 1}\right) - \frac{n}{M\, R(\lambda - 1)} \left(T_D - T_B\right) \,, \tag{10}$$

and

$$\dot{s} = \frac{1}{v} \left[-f_x\, g \left(1 + \frac{k}{\lambda - 1} - s\right) - \frac{n}{M\, R\,(\lambda - 1)} \left(T_D - T_B\right) \right] . \tag{11}$$

3.2 Creep Force Model

The ongoing physical processes in the wheel-rail contact region are of very high complexity and difficult to describe. For instance, the creep force depends on the contact area between the wheel and the rail, its temperature, the surface roughness, as well as environmental conditions such as contamination due to water, oil, dirt, snow and other factors. However, a multitude of measurements showed, that primarily the dependency of the non-dimensional creep force on the longitudinal creepage or creep velocity plays a significant role and obtains the characteristics shown in figure 2 [Vie06]. The model of the non-dimensional creep force in longitudinal direction which is used in this work was suggested by POLACH in [Pol05] and writes

$$f_x(s) = \frac{2\mu}{\pi} \left(\frac{K_A s}{1 + (K_A s)^2} + \arctan\left(K_S s\right) \right) . \tag{12}$$

Here, K_A and K_S are coefficients with values greater than 0 that depend on the parameters of the wheel-rail contact. POLACH assumes that the friction coefficient μ is a function of the creep velocity

$$\mu = \mu_0 \left[(1 - A) \mathrm{e}^{-B|v_s|} + A \right] , \tag{13}$$

where A is the ratio of the limit friction coefficient μ_∞ at infinity creep velocity to the maximum friction coefficient μ_0 at zero creep velocity

$$A = \frac{\mu_\infty}{\mu_0} \,. \tag{14}$$

The coefficient B influences the exponential friction decrease. Figure 4 shows the course of the non-dimensional creep force according to equations (12) and (13) for dry rails (here: $K_A = 250$, $K_S = 100$, $\mu_0 = 0.5$, $A = 0.4$, $B = 0.6$ sec/m). From equation (12) it is clear that for $|s| \to \infty$ follows $|f_x| \to \mu$. With a reasonable choice of K_A and K_S it can be seen from figure 4 that $|f_x| \approx \mu$ already holds for $|s| > 0.1$. Thus, the following approximation of the non-dimensional creep force is assumed for $|s| > 0.1$:

$$f_x(s) \approx \mu_0 \left[(1 - A) \mathrm{e}^{-Bv|s|} + A \right] \cdot \mathrm{sgn}(s) \,. \tag{15}$$

In reality, there is not a single creep force curve that would always occur. Instead, the parameters μ_0, A and B lie in certain ranges:

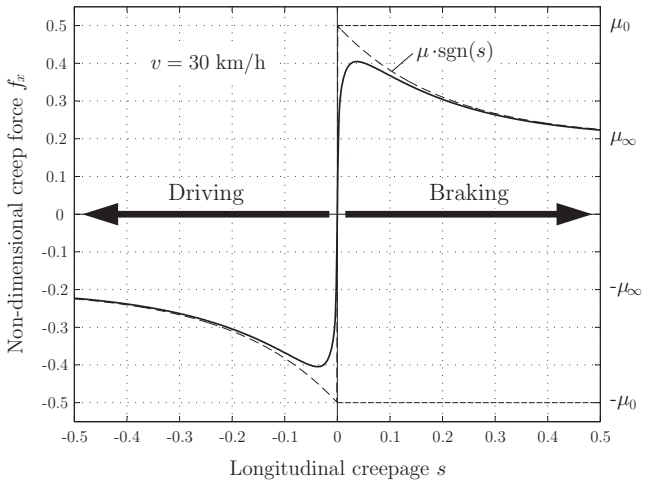

Fig. 4. The POLACH model of the non-dimensional creep force

$$\mu_0 \in [\mu_{0,\min}\,;\, \mu_{0,\max}] \,, \tag{16}$$

$$A \in [A_{\min}\,;\, A_{\max}] \,, \tag{17}$$

$$B \in [B_{\min}\,;\, B_{\max}] \,. \tag{18}$$

Practical wheelslide and wheelskid protection systems must be able to cope with all kinds of possible creep force curves that might emerge during normal operation.

3.3 Actuator Models

Both actuators, the switched reluctance drive and the hydraulic brake, have their own underlying torque control loop. Hence, each actuator possesses a reference torque input and returns the actual torque output value, which is a direct result of the underlying control action. In the following, both actuators are assumed to exhibit a first order lag behaviour which represents the individual torque control dynamics. Thus, for the switched reluctance drive, it holds

$$T_{Drive}\, \dot{T}_D + T_D = T_{D,ref} \,, \tag{19}$$

and for the hydraulic brake

$$T_{Brake}\, \dot{T}_B + T_B = T_{B,ref} \,, \tag{20}$$

with the time constants T_{Drive} and T_{Brake} and the reference torque input variables $T_{D,ref}$ and $T_{B,ref}$. In the following, it is assumed that the switched reluctance drive will be only used for driving and not for braking.

4. DYNAMIC ANALYSIS

First of all, the second order system described by the nonlinear differential equations (1) and (10) is considered. Figure 5 shows the phase portrait for braking ($T_D = 0$, $T_B > 0$) and driving ($T_D > 0$, $T_B = 0$) when started from the initial condition $v = 20$ m/sec, $v_s = 0$ m/sec. The model parameters are $M = 30000$ kg, $n = 4$, $R = 0.46$ m, $k = 1.0$, $\lambda = 1.1$, $\mu_0 = 0.1$, $A = 0.6$, $B = 0.4$ sec/m, $K_A = 250$ and $K_S = 100$.

As long as the maximum (or minimum) of the non-dimensional creep force is not exceeded, braking (or driving) remains stable. For the examples shown in figure 5,

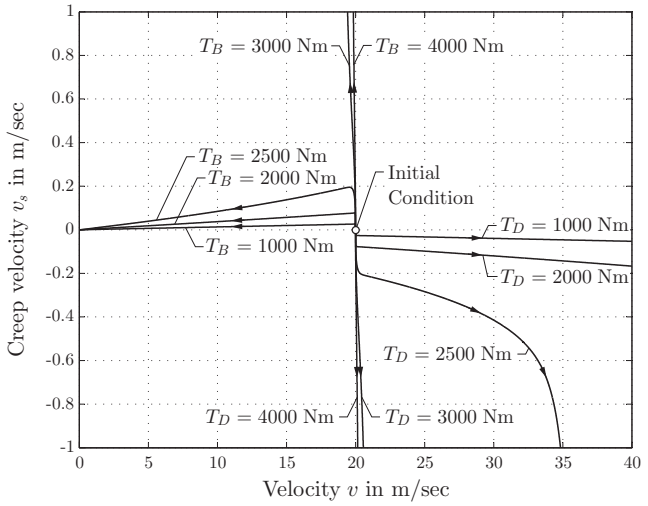

Fig. 5. Phase portrait of the creep velocity vs. velocity for different driving torque and brake torque values

this is the case for $T_B \leq 2500$ Nm and $T_D \leq 2000$ Nm. For $T_D = 2500$ Nm driving is first stable and becomes later unstable since the non-dimensional creep force changes as a function of the creep velocity v_s (see equation 13). Immediately after driving or braking got unstable, the creep velocity v_s changes very quickly whereas the velocity v does not change too much. This fact can be recognised in figure 5 especially for $T_B \geq 3000$ Nm or $T_D \geq 3000$ Nm.

The phase portrait of the second order system represented by the differential equations (1) and (11) is not shown here. But similarly to the creep velocity case shown in figure 5, the longitudinal creepage s changes rapidly while the velocity v remains almost constant after braking or driving became unstable.

As a consequence of these results, a major assumption in this work is that for operating points on the unstable branches of the creep force curve, the vehicle velocity dynamics can be neglected compared to the dynamics of the creep velocity or to those of the longitudinal creepage:

$$\dot{v} \approx 0 \quad . \tag{21}$$

In this particular case, equations (5) and (7) turn into

$$\dot{v}_s = -R\,\dot{\omega}\ , \tag{22}$$

$$\dot{s} = -\frac{1}{v}\,R\,\dot{\omega}\ , \tag{23}$$

where the only difference between $\dot{v}_s$ and $\dot{s}$ is the factor $\frac{1}{v}$ with the parameter v. Again, with equations (2) and (9), $\dot{v}_s$ and $\dot{s}$ become

$$\dot{v}_s = -f_x\,(v_s)\,g\frac{k}{\lambda-1} - \frac{n}{MR(\lambda-1)}\,(T_D - T_B)\ , \tag{24}$$

$$\dot{s} = \frac{1}{v}\left[-f_x\,(s)\,g\frac{k}{\lambda-1} - \frac{n}{MR(\lambda-1)}\,(T_D - T_B)\right]. \tag{25}$$

These relationships write in general

$$\dot{v}_s = f_1(v_s, T_D, T_B)\ , \tag{26}$$

$$\dot{s} = f_2(s, T_D, T_B)\ . \tag{27}$$

In the following, the non-linear model equations (24) and (25) are linearised around an operating point on an unstable branch of the creep force curve and transfer functions are established that describe the behaviour of the system in the vicinity of this operating point. The location of the poles of the transfer functions determine the local stability.

First, the non-linear relationship (27) for the creepage s is linearised around the operating point P $(\dot{s}_0, s_0, T_{D,0}, T_{B,0})$, what results in

$$\Delta\dot{s} = \left.\frac{\partial f_2}{\partial s}\right|_{\mathrm{P}} \Delta s - \frac{n}{M\,R(\lambda-1)v}\,(\Delta T_D - \Delta T_B)\ , \tag{28}$$

with the deviation variables

$$\Delta\dot{s} = \dot{s} - \dot{s}_0\ , \tag{29}$$

$$\Delta s = s - s_0\ , \tag{30}$$

$$\Delta T_D = T_D - T_{D,0}\ , \tag{31}$$

$$\Delta T_B = T_B - T_{B,0}\ . \tag{32}$$

The partial derivative in the operating point is

$$\left.\frac{\partial f_2}{\partial s}\right|_{\mathrm{P}} = \frac{g}{\lambda-1}\underbrace{\left(-k\frac{1}{v}\left.\frac{\partial f_x}{\partial s}\right|_{\mathrm{P}}\right)}_{\sigma(v)}\ . \tag{33}$$

Furthermore, the following abbreviation is introduced

$$\eta = \frac{n}{M\,R(\lambda-1)}\ . \tag{34}$$

Applying the Laplace transform to equation (28) results after a rearrangement in the following relationship

$$S(s) = -\underbrace{\frac{\eta\frac{1}{v}}{s - \frac{g}{\lambda-1}\sigma(v)}}_{G_{WR2}(s)}(T_D(s) - T_B(s))\ , \tag{35}$$

with the transfer function G_{WR2} for the wheel-rail dynamics. The pole is located at

$$s_P(v) = \frac{g}{\lambda-1}\sigma(v)\ . \tag{36}$$

Since the non-dimensional creep force curve has a negative slope (the operating point is on the unstable branches, see figure 4), $\sigma(v)$ is positive and the pole is located in the right-half plane (RHP).

In correspondence to equation (4) and due to the assumption (21), the Laplace-transformed creep velocity $V_s(s)$ and the creepage $S(s)$ are directly related by the constant vehicle velocity v as

$$V_s(s) = v\,S(s)\ . \tag{37}$$

Inserting $S(s)$ from equation (35) into (37) yields the following linear relationship for the creep velocity

$$V_s(s) = -\underbrace{\frac{\eta}{s - \frac{g}{\lambda-1}\sigma(v)}}_{G_{WR1}(s)}(T_D(s) - T_B(s))\ , \tag{38}$$

with the transfer function G_{WR1}, whose pole is located at the same position (36) as the one of G_{WR2}. In addition, it holds

$$G_{WR2} = \frac{1}{v}G_{WR1}\ . \tag{39}$$

Which control variable to take for wheelslide or wheelskid protection, either the longitudinal creepage s or the creep velocity v_s, is a question often raised among practitioners. One result of the analysis above is that under the assumption (21) the location of the unstable pole s_P remains the same, regardless if the longitudinal creepage s or the creep velocity v_s is taken as output of the transfer system. In addition, by investigating equation (36), a well-known fact from experience becomes obvious: the pole s_P is located further to the right for a small λ-value, or in other words, the system is getting "more unstable" for a smaller wheel's moment of inertia I_C.

The value of $\sigma(v)$ and thus the location of the unstable pole depends on the slope of the non-dimensional creep force curve (equation 33). Using the assumption (15) for $|s| > 0.1$, the derivative of the non-dimensional creep force with respect to the longitudinal creepage is

$$\frac{\partial f_x}{\partial s} = \mu_0 (A-1) B\, v\, \mathrm{e}^{-Bv|s|} \ . \tag{40}$$

It is now possible to determine the range of $\sigma(v)$ at a certain velocity v

$$\sigma(v) \in [\sigma_{\min}(v)\ ;\ \sigma_{\max}(v)] \ , \tag{41}$$

where the longitudinal creepage in the operating point s_0 may lie in the domain $|s_0| \in [s_{\min,0}\ ;\ s_{\max,0}]$ with $s_{\min,0} \geq 0.1$. The factor k that accounts for a possible change in the normal force may lie in the range $k \in [k_{\min}\ ;\ k_{\max}]$. The lower bound of (41) is then

$$\sigma_{\min}(v) = \begin{cases} Z_{\min} B_{\min} \mathrm{e}^{-B_{\min} s_{\max,0} v} & ;\ v \leq v_T \\ Z_{\min} B_{\max} \mathrm{e}^{-B_{\max} s_{\max,0} v} & ;\ v > v_T \end{cases} \tag{42}$$

with

$$v_T = \frac{\ln(B_{\min}) - \ln(B_{\max})}{s_{\max,0}\,(B_{\min} - B_{\max})} \tag{43}$$

and

$$Z_{\min} = k_{\min}\, \mu_{0,\min}\, (1 - A_{\max}) \ . \tag{44}$$

The upper bound of (41) results in

$$\sigma_{\max}(v) = \begin{cases} Z_{\max} B_{\max} \mathrm{e}^{-B_{\max} s_{\min,0} v} & ;\ v < \frac{1}{B_{\max} s_{\min,0}} \\ Z_{\max} B_{\min} \mathrm{e}^{-B_{\min} s_{\min,0} v} & ;\ v > \frac{1}{B_{\min} s_{\min,0}} \\ Z_{\max} \frac{1}{s_{\min,0} v} \mathrm{e}^{-1} & ;\ \text{otherwise} \end{cases} \tag{45}$$

with

$$Z_{\max} = k_{\max}\, \mu_{0,\max}\, (1 - A_{\min}) \ . \tag{46}$$

For a given velocity range $v \in [v_{\min}\ ;\ v_{\max}]$, the pole variation for an entire braking or driving procedure is finally

$$s_P \in \left[\frac{g}{\lambda - 1} \sigma_{\min}(v_{\max})\ ;\ \frac{g}{\lambda - 1} \sigma_{\max}(v_{\min}) \right] \ . \tag{47}$$

This range of the pole location needs to be considered in the following controller design.

5. CONTROLLER DESIGN

First of all, the appropriate control variable must be chosen. In this approach, the longitudinal creepage s is taken as control variable for wheelslide protection (braking). As mentioned above, s lies in a range between 0 (purely rolling wheel) and 1 (wheel lock-up) during braking. Hence, by controlling s, the ratio between these two extreme states can be directly influenced. Furthermore, [UIC05] specifies that a wheelslide protection system should be able to stabilise the braking down to a velocity of about 3 km/h before the full and unaffected brake torque must be applied to the wheel. Thus, the fact that s is not defined for $v = 0$ is of no great matter for wheelslide protection. However, in the case of wheelskid protection (driving), very often the wheel skidding has to be prevented at extremely low velocities. As a consequence, the creep velocity v_s is preferred as control variable for wheelskid protection in this work.

From equation (19), the transfer function G_D of the switched reluctance drive can be determined as

$$G_D(s) = \frac{T_D(s)}{T_{D,ref}(s)} = \frac{1}{T_{Drive}\, s + 1} \ . \tag{48}$$

The transfer function G_B of the hydraulic brake is found from equation (20)

$$G_B(s) = \frac{T_B(s)}{T_{B,ref}(s)} = \frac{1}{T_{Brake}\, s + 1} \ . \tag{49}$$

The overall transfer function which describes the dynamic behaviour in the wheelskid case is given by the serial connection

$$G_{SK}(s) = \frac{V_s(s)}{T_{D,ref}(s)} = -G_D(s)\, G_{WR1}(s) \ . \tag{50}$$

Similarly, the dynamic behaviour of the sliding wheel is represented by

$$G_{SL}(s) = \frac{S(s)}{T_{B,ref}(s)} = G_B(s)\, G_{WR2}(s) \ . \tag{51}$$

In this approach, the controller design is based on the consideration of the pole location s_P which is furthest to the right in the RHP. Hence, controllers are to be designed that are able to stabilise the two systems

$$G_{SK}(s) = -\frac{1}{T_{Drive}\, s + 1} \cdot \frac{\eta}{s - \frac{g}{\lambda - 1} \sigma_{\max}(v_{\min})} \tag{52}$$

and

$$G_{SL}(s) = \frac{1}{T_{Brake}\, s + 1} \cdot \frac{\frac{\eta}{v_{\min}}}{s - \frac{g}{\lambda - 1} \sigma_{\max}(v_{\min})} \ . \tag{53}$$

A key technique used to stabilise loops with an unstable plant is a lead compensator. A controller of the form

$$G_C(s) = K_R \frac{T_V s + 1}{T s + 1} \ , \quad T_V > T > 0 \tag{54}$$

is able to stabilise both, a closed loop including G_{SK} from equation (52) and one including G_{SL} from equation (53). As a rule of thumb, the controller parameters K_R, T_V and T have to be chosen in such a way that the bandwidth of the control system extends beyond the frequency of the highest frequency unstable pole (see citations in [Stü06]). Hence, the bandwidth must be greater than $\frac{g}{\lambda - 1} \sigma_{\max}(v_{\min})$.

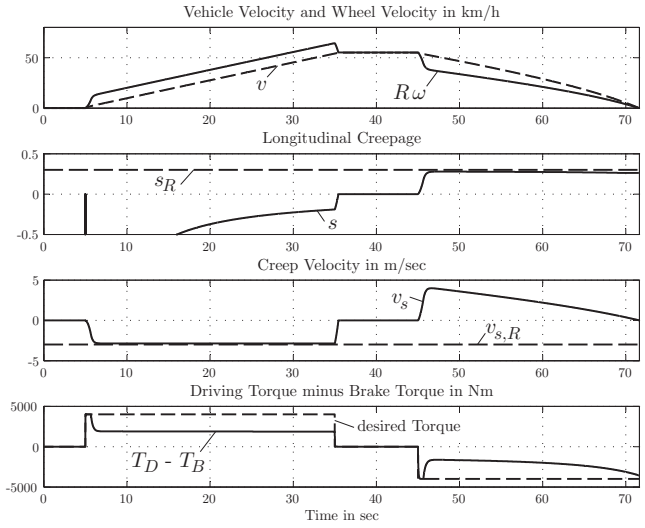

Fig. 6. Creep velocity and creepage control with creep force parameters $\mu_0 = 0.1$, $A = 0.4$ and $B = 0.6$ sec/m

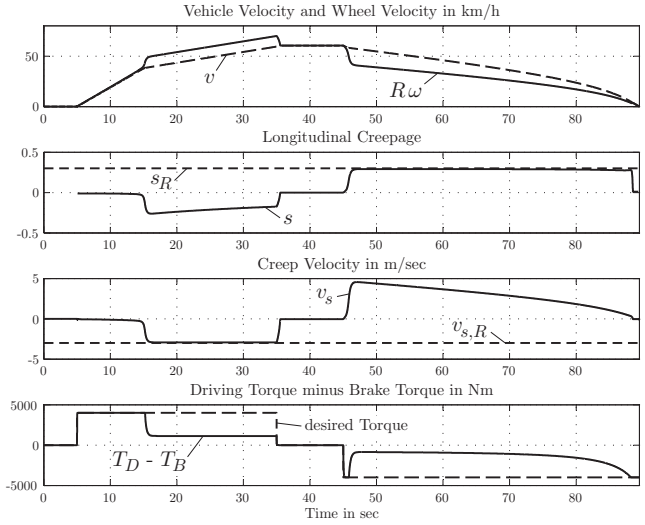

Fig. 7. Creep velocity and creepage control with creep force parameters $\mu_0 = 0.15$, $A = 0.15$ and $B = 0.95$ sec/m

Simulation results are shown in figures 6 and 7. In the chosen simulation scenario, the train driver applies first a driving torque $T_{D,des} = 4000$ Nm and later a brake torque $T_{B,des} = 4000$ Nm while running on slippery rails. The difference $T_{D,des} - T_{B,des}$ is called desired torque and shown as a dashed line in the lowest subplot of the figures 6 and 7. For wheelskid protection, a creep velocity reference value of $v_{s,R} = -3$ m/sec is chosen. In the wheelslide protection case, $s_R = 0.3$ is taken as creepage reference value. In figure 6, common nominal parameter values are taken for the non-dimensional creep force curve (15) ($\mu_0 = 0.1$, $A = 0.4$, $B = 0.6$ sec/m). As can be seen from the simulation results, the creep velocity control during driving and the creepage control during braking are both stable. The scenario shown in figure 7 illustrates driving and braking under frictional conditions that are even more critical due to a steeper slope of the non-dimensional creep force curve ($\mu_0 = 0.15$, $A = 0.15$ and $B = 0.95$ sec/m). However, these values of μ_0, A and B still lie within the parameter ranges that were considered in the determination of the pole variation (47). Since the creep velocity controller and the creepage controller are both given in the form (54) and were both designed with regard to (47), the control is stable, even in the critical case depicted in figure 7.

6. CONCLUSION

The wheelskid and wheelslide protection task for a single wheel with an integrated drive and brake system was considered. By using mathematical models, a dynamic analysis was performed which showed, that for operating points on the unstable branches of the creep force curve the system has an unstable pole that depends on the shape of the creep force curve. For a given range of the creep force curve parameters, the possible locations of the pole in the right-half plane were determined and based on this result, a conventional controller structure was suggested for both, creep velocity control and creepage control, that was able to stabilise the system, even for critical frictional conditions. Further research should investigate the parameter value changes of the creep force curve during driving or braking with respect to altering rail conditions over the track length.

ACKNOWLEDGEMENTS

The authors would like to thank the German Research Foundation (DFG) for the financial support.

REFERENCES

[Ger06] J. Germishuizen, A. Jöckel, T. Hoffmann, M. Teichmann, L. Löwenstein, and F. v. Wangelin. Syntegra - Next Generation Traction Drive. *Speedam* 2006, Taormina, Italy.

[Her07] M. Hermanns, and T. Dellmann. Progress in the design of SDBM. Presentation at *The Fourth SDBM Colloquium*, July 6, 2007, Aachen, Germany.

[Stü06] T. Stützle, U. Viereck, A. Stribersky, W. Rulka, M. Enning, and D. Abel. Creepage Control for Use in Wheelslide Protection Systems. In: *Proceedings of the 11th IFAC Symposium on Control in Transportation Systems*, August 29-31, 2006, Delft, The Netherlands.

[UIC05] UIC, Union Internationale des Chemins de Fer. Brakes - Regulations concerning the construction of the various brake components - Wheel slip prevention equipment. *UIC-Kodex* 541-05 VE. Paris, France, 2005.

[Wu98] M.C. Wu, L.C. Lee and M.C. Shih. Neuro-Fuzzy Controller Design of the Anti-Lock Braking System. *JSME International Journal - Series C*, 41(4):836–843, 1998.

[Vie06] U. Viereck, T. Stützle, W. Rulka and A. Stribersky. Analysis of the braking performance of a rail vehicle emphasizing mechatronic components. In: S. Bruni and G. Mastinu, editors, *The Dynamics of Vehicles on Roads and on Tracks, Proceedings of the 19th IAVSD Symposium*, August 28 - September 2, 2005, Milan, Italy. Supplement to Vehicle System Dynamics, volume 44, pages 823–833, 2006.

[Pol05] O. Polach. Creep forces in simulations of traction vehicles running on adhesion limit. *Wear*, 258:992–1000, 2005.